Surface & Coatings Technology 398 (2020) 126127

Contents lists available at ScienceDirect

Surface & Coatings Technology

journal homepage: www.elsevier.com/locate/surfcoat

Microstructure, corrosion behaviour and thermal stability of AA 7150 after ultrasonic shot peening

Qingqing Sun[a,b,**], Qingyou Han[b], Shuai Wang[a,*], Rong Xu[c]

[a] Department of Mechanical and Energy Engineering, Southern University of Science and Technology, Shenzhen, Guangdong 518055, China
[b] School of Engineering Technology, Purdue University, West Lafayette, IN 47907, United States of America
[c] School of Mechanical Engineering, Purdue University, West Lafayette, IN 47907, United States of America

ARTICLE INFO

Keywords:
Surface nanocrystallization
Exfoliation corrosion
Post ageing
Surface softening
AA 7150

ABSTRACT

Microstructure, corrosion behaviour and thermal stability of ultrasonic shot peened AA7150 were studied in this work. After ultrasonic shot peening, exfoliation susceptibility decreases, intergranular corrosion is inhibited for both normal and transverse planes, pitting potential shifts to the positive direction. The enhanced localized corrosion resistance is attributed to the formation of equiaxed nano-grains on surface layer. Pre-existing ageing-induced η′ and η precipitates dissolved immediately after shot peening, however, after 18 months' natural ageing, nanograined precipitates with more coarsened size than pre-existing ones, re-precipitate on the peened surface layer and leads to surface softening.

1. Introduction

In the last several decades, surface severe plastic deformation (S^2PD) has been used to modify alloys' surface layer for the purpose of improving surface-related properties like surface hardness, corrosion and wear [1–4]. S^2PD is one technique that can induce severe plastic deformation on the surface of alloys, resulting in grain size refinement, surface hardening, high level of compressive residual stress and introduction of high density of defects such as dislocation and vacancy [5–11]. The family of S^2PD consists of air blast shot peening [12], ultrasonic shot peening (USSP) [13,14], ultrasonic impact peening [15,16], laser shock peening [17], sand blasting [18], ball burnishing [19], friction stir [20] and so on.

Corrosion performance of alloys subjected to surface mechanical treatments has been extensively studied, but most of the literature has been focused on electrochemical corrosion behaviours [7,19,21–25]. It has been argued that one should pay more attention on localized corrosion behaviours instead of on uniform corrosion performances which derived from electrochemical characterization methods such as open circuit potential, electrochemical impedance spectra and polarization [26,27]. This is because corrosion is alloy-dependent and environment-dependent and in some cases electrochemical results can be misleading and localized corrosion is more important and more frequent for some alloy systems [26,27]. For instance, one of localized corrosion forms, exfoliation corrosion, has been shown to deteriorate significantly the fatigue life of alloys [28], but can't be precisely reflected by electrochemical methods. It's well recognized that the studied 7000 series Al alloys in this paper are sensitive to exfoliation corrosion. Actually, among the various corrosion phenomena (pitting corrosion, intergranular corrosion, stress-corrosion cracking), exfoliation corrosion is particularly relevant to plates presenting grains of large aspect ratio [29]. Surface mechanical treatments can alter the surface texture and change aspect ratio dramatically, thus it is worthy to investigate the exfoliation performance of S^2PD treated 7000 series Al alloys.

Though the hardness, wear, fatigue and corrosion behaviours can be greatly improved by grain refinement, the introduced high density of defects such as dislocations and grain boundaries provides a strong driving force for grain coarsening, accompanied by property degradation. Therefore, thermal stability of nanograined metals is a great concern for their applications. It was reported that below a critical size (70 nm), nanometer-sized grains in pure copper and nickel produced by SMGT (surface mechanical grinding treatment) exhibit notable thermal stability [30]. Nanograined structure in pure copper and pure nickel stays stable at 250 and 600 °C, respectively. For shot peened SS316L, grain size does not show an obvious growth during post annealing at 600 °C [31]. Compared with Fe, Cu, Ni and Ti alloy systems, due to the low melting temperature of Al alloys, thermal stability property might be unique for Al alloys subjected to severe plastic deformation. For

* Correspondence to: Q. Sun, Department of Mechanical and Energy Engineering, Southern University of Science and Technology, Shenzhen, Guangdong 518055, China.
** Corresponding author.
E-mail addresses: sunqq@sustech.edu.cn (Q. Sun), wangs@sustech.edu.cn (S. Wang).

https://doi.org/10.1016/j.surfcoat.2020.126127
Received 27 May 2020; Received in revised form 15 June 2020; Accepted 27 June 2020
Available online 29 June 2020

example, Al-Cu supersaturated solid solution can be further hardened under room temperature through the precipitation of nanograined $AlCu_2$, which termed as natural ageing treatment. Mazilkin et.al found that Al-Zn and Al-Mg supersaturated solid solutions decompose after high pressure torsion (HPT) [32,33]. The Hall–Petch hardening due to grain refinement competes with softening effect caused by the decomposition of a supersaturated solid solution, leading to a net softening for the Al-Zn and Al-Mg binary alloys [32,33]. 7000 series Al alloys are typical alloys that can be precipitation hardened by the introduction of η′ and η precipitates during artificial ageing at the temperature of 120–200 °C. After USSP and grinding, pre-existing ageing-induced η′ and η precipitates of 7000 series alloys are found dissolving into Al matrix and results in a supersaturated solid solution, due to the fact that severe plastic deformation can extend solid solubility of alloying elements in the Al matrix. The phenomenon has been reported on the AA 7150 [34] and AA 7055 [35] subjected to grinding and AA 7075 [36] subjected to USSP. Supersaturated solid solution together with the high stored energy caused by USSP treatment, are expected to lead to an unsatisfactory thermal stability. In this work, the post-ageing induced decomposition of USSP treated AA7150 supersaturated solid solution and its effect on surface hardness will be investigated.

2. Experimental

2.1. Materials and USSP setup

The studied material is a rolled 7150-T7751 Al alloy plate received from Alcoa. Chemical composition and 3D optical microstructure of AA 7150 and details of USSP are shown elsewhere [26]. The plate was cut into specimens with the dimension of 6 × 50 × 50 mm^3 before USSP treatment. The S440 stainless steel with diameter of 3–5 mm and 3 mm Ø SiN balls were used as shot peening media. A typical USSP treated sample is marked with “U-deformed thickness”, where deformed thickness can be determined by optical observation and has a unit of μm. Both ND (Normal direction) and TD (transverse direction) planes of AA7150 were subjected to USSP. In order to study the thermal stability of peened alloy, post-ageing, i.e., natural ageing up to 18 months, was followed after shot peening treatment.

2.2. Optical microstructure

After etched by Keller's reagent (i.e., 95 mL of H_2O + 2.5 mL of HNO_3 (70%) + 1.5 mL of HCl (37%) + 1.0 mL of HF (48%)), optical micrographs of cross-sections of peened alloys were characterized with Leica optical microscopy. Cross-sections of peened alloys were obtained by polishing the sample after embedded into epoxy, with a surface finishing using 1 μm Al_2O_3.

2.3. Corrosion tests

Based on ASTM standard G34-01, accelerated exfoliation corrosion (EXCO) test was performed in 4 mol/L NaCl + 0.5 mol/L KNO_3 + 0.1 mol/L HNO_3 solution at 25 ± 3 °C for 24 h. The susceptibility to exfoliation of alloys is determined by visual examination. USSP sample was treated using stainless steel balls with diameter of 4 mm to have a deep affected thickness (~150 μm). After exfoliation test, the cross sections of samples were etched by Keller's reagent and then characterized using optical microscopy. According to ASTM standard G110-92, intergranular corrosion (IGC) tests were conducted in 57 g/L NaCl + 10 mL/L H_2O_2 solution with solution volume (mL)/alloy area (cm^2) ratio 15:1. The exposures were conducted under room temperature with periods of 24, 48, 72 and 96 h, with fresh solution replaced every 24 h for exposures more than 1 day. After exposure, each specimen was ultrasonically rinsed in water and cross-sectional images were taken using Leica optical microscope to measure the depth of IGC. Average IGC depth was calculated in a length scale of at least 50 mm for each sample. Polarization measurements of alloys were conducted on VersaSTAT 3 potentiostat/galvanostat in naturally aerated 3.5 wt% NaCl solution at room temperature. A three-electrode cell was used, with 1.0 cm^2 testing material as working electrode, platinum gauze as counter electrode and saturated calomel (SCE) electrodes as reference electrode. Polarization curves were obtained at a scan rate of 0.2 mV/s in a Faraday cage. Also should be noted is that all the corrosion tests (including exfoliation, intergranular and electrochemical corrosion) samples in this paper were within one month after USSP treatments.

2.4. Thermal stability

After USSP, samples were naturally ageing treated for 18 months before thermal stability tests. Post-ageing induced microstructure and initial microstructure without USSP treatment were studied using transmission electron microscopy (TEM) and XRD. TEM specimens were prepared using the focused ion beam (FIB) in situ lift-out technique in a FEI Helios NanoLab field emission gun (FEG) dual beam microscope. A voltage of 2 kV and a current of 23 pA were used during the final thinning step to minimize the damage caused by the ion beam. TEM images and HAADF-EDS elements mapping of AA7150 samples were collected with an FEI/Talos F200X instrument operated at 200 kV. XRD patterns were performed using a Bruker D-8 Focus X-ray diffractometer with CuKα radiation at scanning rate of 4°/min to determine the surface alloy phase constituent changes before and after USSP.

2.5. Hardness

Keysight G200 Nano Indenter was employed to measure the hardness and Young's modulus of surface layer of USSP treated AA 7150 (SiN balls with diameter of 3 mm were chosen for the purpose of obtaining sample with clean surface). Note that there are 15 months-long natural ageing between USSP treatment and indentation test. Indentation tests were performed using Berkovich tip at a constant strain rate of 0.05 s^{-1}. Poisson ratio of 0.3 and 5 s peak hold time were used. The hardness and modulus are determined by using Eqs. (1) and (2), respectively.

$$H = \frac{P_{max}}{A} \tag{1}$$

$$E_r = \frac{\sqrt{\pi}}{2\beta}\frac{S}{\sqrt{A}} \tag{2}$$

where P_{max} is the maximum applied stress, A is contact area, E_r is elastic modulus, β is a constant value which is determined by the shape of tip and S is the elastic stiffness.

3. Results

3.1. Optical microstructure

Cross-sectional optical micrographs of peened 7150 Al alloys are shown in Fig. 1. For sample U-150 which treated using steel shots, the thickness (~150 μm) of grain distortion and refinement is quite large. By contrast, for sample U-40 treated by SiN balls, the deformation affected area is much smaller (about 40 μm), this is because larger shot distance, shorter peening duration and much lighter SiN shots imposed on workpiece. Below the deformed layer is the substrate alloy, from which the initial microstructure prior to USSP can be seen. The initial alloy has elongated rolling grains with width of ~10 μm, within which subgrains with size of 2–3 μm distributed.

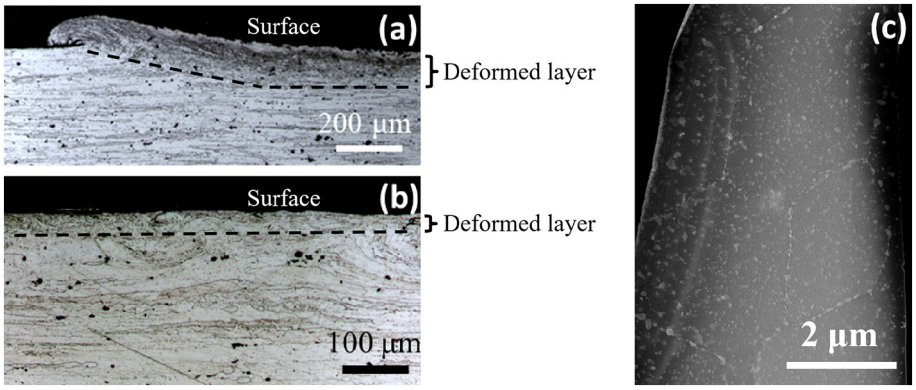

Fig. 1. Cross-sectional optical micrographs of peened 7150 Al alloys: (a) High energy (U-150); (b) Low energy (U-40). (c) TEM images of the initial alloy prior to USSP showing the presence of subgrains with size of 2– 3 μm.

3.2. Exfoliation corrosion

Exfoliation corrosion was tested in standard EXCO solution at 25 ± 3 °C for 24 h. After exfoliation test, alloy surfaces of untreated and USSPed sample are respectively shown in Fig. 2a and b. The USSP treatment parameter of alloy for exfoliation corrosion test is U-150 using steel balls. Using un-aided eyes, the susceptibility of exfoliation corrosion was found decreasing from EC to EB after ultrasonic shot peening treatment.

3.3. Intergranular corrosion

IGC testing for both ND and TD planes was conducted and the results are exhibited in Fig. 3. For untreated condition, IGC was present for both ND and TD samples (Fig. 3a and b). The corrosion depth found in TD sample is much deeper than that in ND sample, indicating that IGC propagates along elongated grain boundaries. Surprisingly, for USSP treated condition, IGC was completely inhibited in both ND and TD samples, as shown in Fig. 3c and d. Statistically, as depicted in Fig. 3e and f, average IGC depths were calculated and compared after immersing into testing solution for a certain duration. Note that IGC testing solution was replaced with fresh one every 24 h to make sure that the solution aggressive enough for IGC test. From these statistical results, we find that during 96 h long immersion, IGC never happens in both USSP-ND and USSP-TD samples. This is a strong evidence for the statement that USSP can greatly enhance IGC resistance of AA 7150, implying that high energy USSP is a potential powerful tool for localized corrosion prevention engineering.

3.4. Electrochemical corrosion

Fig. 4 shows polarization curves of AA 7150 with and without USSP treatments performed in naturally aerated 3.5 wt% NaCl solution at room temperature. For high energy group of samples (U-70 and U-150, the thickness of deformation layer is more than 50 μm), pitting potentials are absent from polarization curves, as shown in Fig. 4a. While for low energy group (U-5 and U-15, the thickness of deformation layer is less than 20 μm), pitting potentials are clearly evident in the polarization curves, Fig. 4b. Pitting potential shifts to the more anodic direction after USSP (E_{pit} is −0.775, −0.755 and −0.739 V_{SCE} for untreated, U-5 and U-15, respectively), indicating an improved initiation resistance of localized corrosion.

It can be seen that for both high energy group (Fig. 4a) and low energy group (Fig. 4b), corrosion current densities of peened alloys are comparable or even slightly higher, compared to those of their untreated counterparts. Current density results seem like showing a disagreement with improved exfoliation corrosion and IGC resistance, actually this is due to the deceptive effect caused by the surface contamination induced during USSP treatment. We further conducted polarization tests after immersing samples into 57 g/L NaCl + 10 mL/L H_2O_2 solution for 1 h and 2 h. Note that surface contamination layer would be totally exfoliated after 30 min immersion into 57 g/L NaCl + 10 mL/L H_2O_2 solution, so that contamination layer's deceptive effect can be avoided [27]. Tafel plots shown in Fig. 5 indicate that corrosion current density of USSPed sample, after pre-immersion, becomes lower than that of the untreated counterpart. In addition, obvious pitting potentials appears after 2 h pre-immersion, and the E_{pit} value of USSPed sample is more positive.

3.5. Thermal stability

After USSP treatment, average grain size in the topmost layer of AA 7150 was reduced from micrometer-scale down to 30–60 nm as indicated by XRD and TEM [26], along with a large number of defects

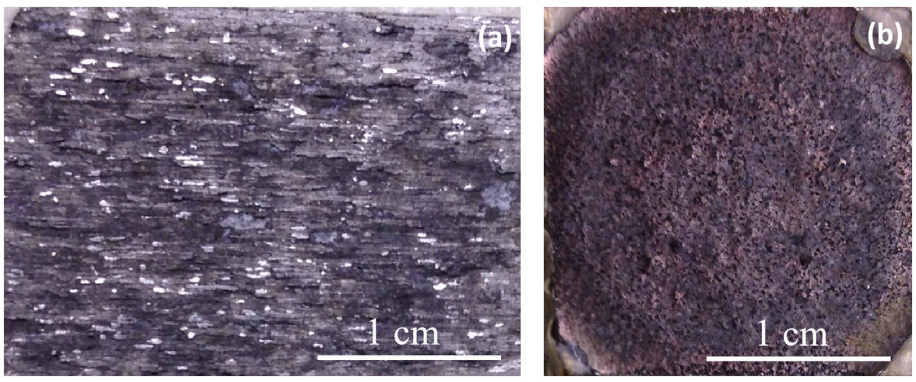

Fig. 2. Alloy surfaces after exfoliation test: (a) Untreated sample; (b) USSP treated sample (U-150).

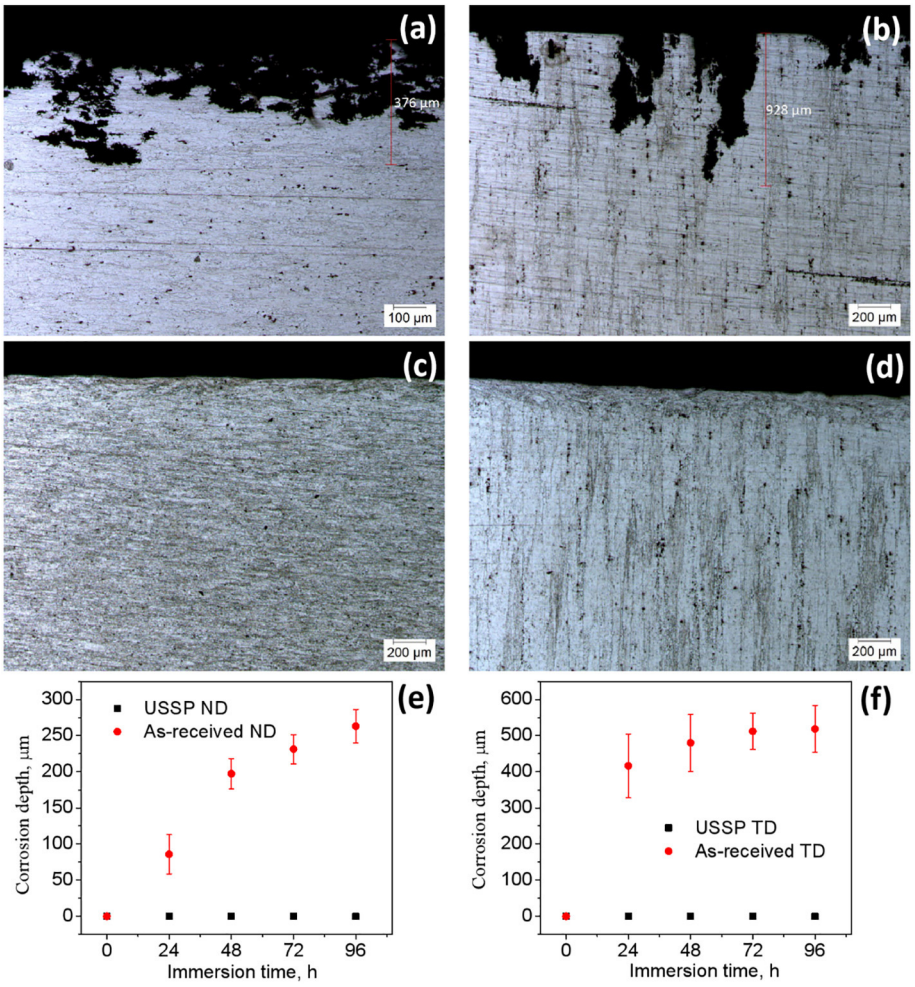

Fig. 3. The representative cross-sectional images of as-received ND plane (a), as-received TD plane (b), USSPed ND plane (c), USSPed TD plane (d) after exposure in 57 g/L NaCl + 10 mL/L H_2O_2 solution; corrosion depth statistics as a function of immersion time for ND plane (e) and TD plane (f). Testing solution was replaced with fresh one every 24 h. USSP parameter is U-150.

induced by heavy deformation. Fig. 6 shows HAADF images and the corresponding diffraction patterns of peened and 18 months naturally aged AA 7150 at different depths. Even after 18 months natural ageing, the USSPed topmost surface still are characterized with nanograined grains (~50 nm in average), seen in Fig. 7a. This indicates that the nanocrystalline Al grains formed by USSP treatment didn't have a significant growth during long-term natural ageing treatment.

7000 series Al alloys are precipitation hardenable and the high strength of 7000 series Al alloys is mainly attributed to the ageing-induced η′ and η precipitates which inhibit the movements of dislocations. XRD results in Fig. 7 proves that pre-existing ageing-induced η′ and η precipitates of AA 7150 dissolved into matrix or refined to very small scale (below 5 nm) after USSP treatment. Whether η′ and η precipitates completely dissolve into matrix cannot be determined by XRD only, further TEM work is needed. Note that XRD tests were conducted on TD plane of alloy after USSP processing and the following 1 month natural ageing, which are in agreement with ND plane results [26]. Therefore, microstructure homogenization on surface peened layer was achieved at least for the first month after USSP treatment. Pre-existing ageing-induced η′ and η precipitates were also found dissolved for AA 7055 [35] after surface abrasion, for AA 7075 [36] after ultrasonic shot peening and for AA 7150-T651 [34] during machining.

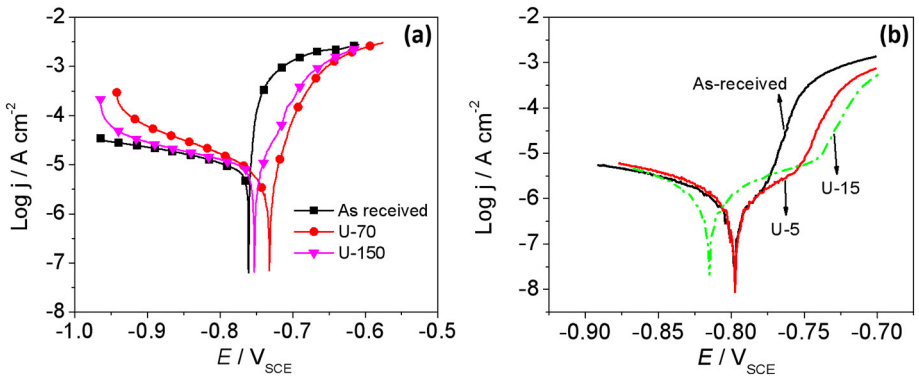

Fig. 4. Tafel plots of AA 7150 with and without USSP treatments performed in naturally aerated 3.5 wt% NaCl solution at room temperature: (a) High energy group: U-70 and U-150; (b) Low energy group: U-5 and U-15. Note that the curves of as-received shown in subpanels a and b are different because they are conducted in different batches.

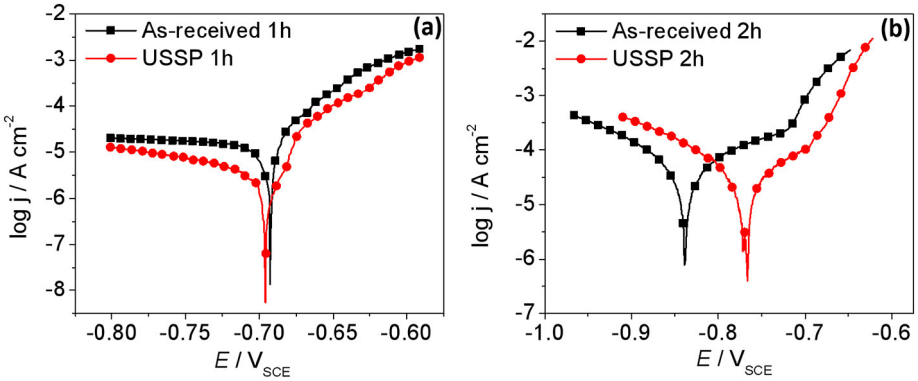

Fig. 5. Tafel plots of AA 7150 without and with high energy USSP treatment (U-150) performed in naturally aerated 3.5 wt% NaCl solution at room temperature: (a) 1 h pre-immersion; (2) 2 h pre-immersion.

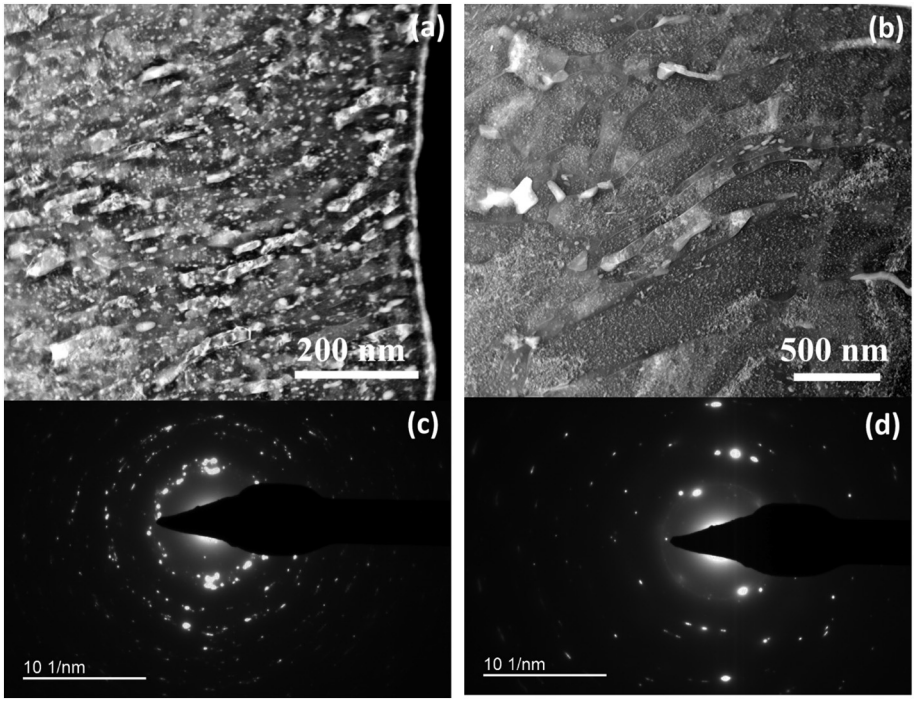

Fig. 6. HAADF images and the corresponding diffraction patterns of AA 7150 (USSP treatment and 18 months' natural ageing): (a) (c) ~2 μm to surface; (b) (d) ~15 μm to surface. USSP parameter is U-40 using SiN balls.

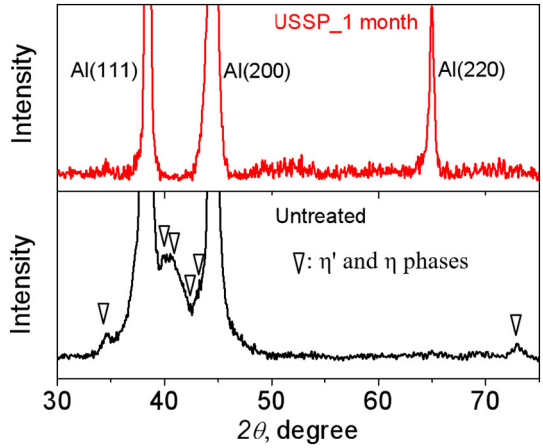

Fig. 7. XRD patterns of AA 7150 alloys with and without USSP treatment & post ageing.

Different with the relatively good thermal stability of nanocrsytalline Al matrix, the η′ and η precipitates are found re-precipitated during natural ageing. Actually, natural ageing is a common phenomenon for Al alloys due to the relative low melting temperature of Al. After USSP treatment, massive stored strain energy and supersaturated solution due to the dissolution of η′ and η precipitates result in a metastable system, thus precipitates are expected to re-precipitate easily. The peened sample was aged at room temperature for 18 months, and then the precipitates were investigated by combining FIB machining and STEM techniques. As shown in Fig. 6a and b, the re-precipitation phenomenon is evident in the vicinity of surface. High magnification images shown in Fig. 8 indicate that the particle size of re-precipitated precipitation (10–25 nm) is much larger than that of pre-existing ageing-induced precipitates (5–10 nm). In addition, as can be seen in Fig. 9, the re-precipitated particles are enriched in Zn, Mg and Cu, which is the same as pre-existing η precipitates [37].

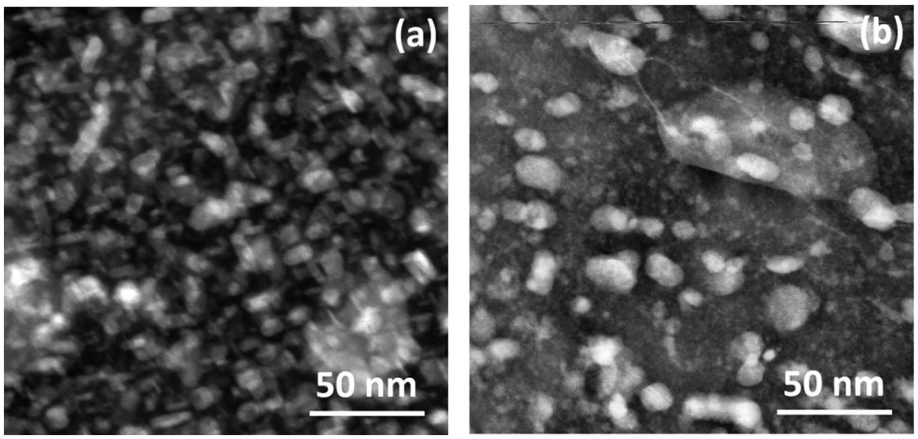

Fig. 8. HAADF images of precipitations of AA 7150: (a) untreated; (b) USSPed &18 months' natural aged samples. USSP parameter is U-40 using SiN balls.

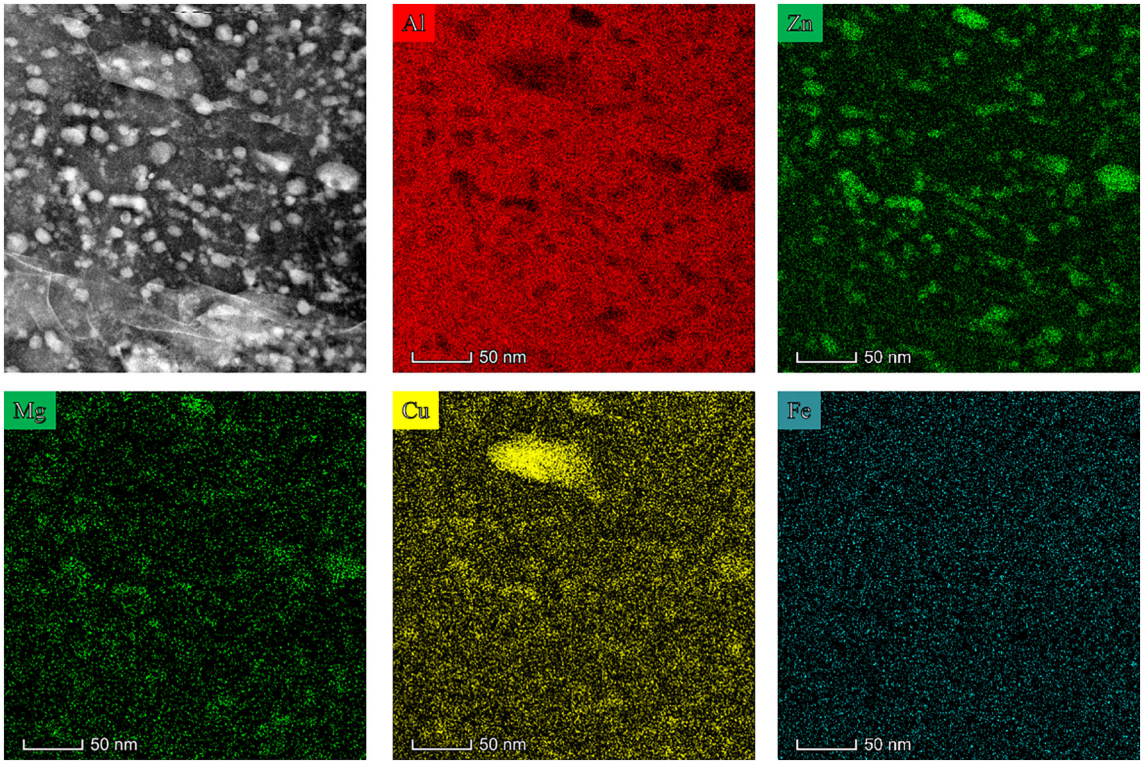

Fig. 9. HAADF images of AA7150 (U-40 &18 months' natural aged) and the corresponding elements map.

4. Discussion

4.1. Relationship between corrosion and microstructure

In standard IGC testing solution, for both ND and TD planes subjected to USSP, IGC does not happen even after 96 h' immersion (Fig. 3). IGC was found to propagate along grain boundaries, especially along elongated grain boundaries. The same elimination effect of USSP on IGC for both ND and TD planes is due to the same microstructure formed after USSP treatments. As can be seen in Fig. 10, (220) crystallographic plane is the preferential orientation for ND plane of as-received state, while for TD plane it is (200) plane. But after ultrasonic shot peening, the preferential orientations disappeared for both ND and TD, as stated by the relative XRD intensities of different crystallographic planes. Actually it is an indicator of equiaxed grains presenting on alloy surface layer after shot peening, for both ND and TD planes. The calculated grain size and microstrain for TD plane is 26.8 ± 5.1 nm and 1.73 ± 0.06%, respectively, which are similar with ND results [27]. We believe it is due to the high IGC resistance of equiaxed nanograined grains that IGC can be completely inhibited by USSP treatment. IGC is easily initiates and propagates along micro-scale elongated grains of Al-Zn-Mg-Cu alloys, especially when η precipitates distribute continuously on the grain boundary [38,39]. The dissolving of η precipitates makes the grain boundaries less sensitive to IGC and the nearly random texture cut off the rapid propagation path of IGC.

Exfoliation susceptibility decreases from EC to EB after ultrasonic shot peening treatment, as shown in Fig. 2. A number of phases are believed to play a role in exfoliation of Al alloy [29]: (a) Sensitivity to IGC; (b) Wedge effect on the grain lift-up due to the accumulation of corrosion products; (c) SCC of the alloy; (d) Hydrogen embrittlement of Al alloy. We believe the enhancement of exfoliation corrosion resistance is mainly attributed to grain refinement and distortion effects caused by USSP. In general, exfoliation corrosion propagates rapidly along the elongated grain boundaries, namely, along grains with large

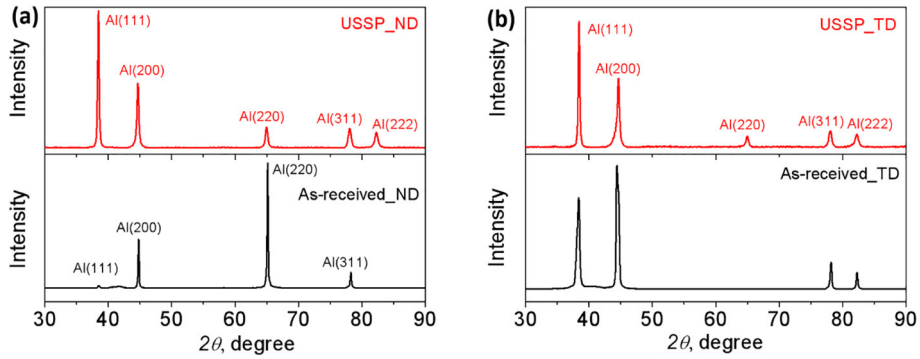

Fig. 10. X-ray diffraction patterns of different planes of AA 7150: (a) ND plane [27]; (b) TD plane. USSP parameter is U-150.

aspect ratio because of large wedge effect. Grain distortion caused by USSP leads to nearly random texture which cuts off the quick propagation paths for exfoliation corrosion. Thus, the improvement in exfoliation corrosion resistance of AA 7150 is achieved. Note that all corrosion tests in this work were done within one month after USSP, thus microstructure homogenization on the surface peened layer also plays an important role in the enhancement of localized corrosion resistance due to the reduced galvanic interaction effect. In addition, high level of compressive residual stress would be introduced on the surface layer after USSP, which can retard the wedge effect of corrosion products and thus improving the resistance of exfoliation corrosion.

4.2. Thermal stability and hardness

There are four main strengthening mechanisms for metals and alloys: solid solution strengthening, precipitation hardening, strain hardening and grain boundary strengthening. Surface severe plastic deformation is a well-known technique that can harden alloy surface layer, mainly due to the introduction of high densities of defects such as dislocation, stacking fault and grain boundaries [5,6,13,40]. For instance, if merely taking Hall-Petch relationship into consideration, the strength of peened AA 7150 is expected to be much higher than that of the untreated counterpart. However, during long-term natural ageing, coarsening of precipitation is evident, which is a softening factor for Al alloy. Therefore, due to the contradictory factors presented, it is difficult to calculate or predict the hardness changes.

Load-displacement curves of AA 7150 substrate and peened surface layer (with 15 months-long natural ageing) are shown in Fig. 11a, from which hardness and modulus can be determined. Note that the peened alloy is treated using SiN shots (U-40), for the purpose of avoiding the introduction of thick Fe-rich contamination layer which might confound the hardness results of deformed layer [27]. Hardness gradually decreases when approaching to the peened surface, as can be seen from Fig. 11b. Correspondingly, the yield strength decreases from ~700 MPa to ~300 MPa. Same with strength, Young's modulus also gradually decreases as approaching the peened surface, Fig. 11c. Obviously, our finding on surface softening is contradictory with many literature work [1,9,41,42].

Comparing the surface layer and the substrate, elements in solid solution can be seen having a marginal difference. Due to the fact that coarsening of precipitates during long time natural ageing is accompanied by the annihilation of dislocations, thus the dislocation density in different depths has no major difference. Therefore, the hardness change is mainly attributed to the change in grain boundary strengthening (Hall–Petch mechanism) and precipitation hardening (Orowan bypass mechanism) factors.

The relationship of the mechanical properties and average grain size as has described as the Hall–Petch equation:

$$\sigma = \sigma^{o} + kd^{-0.5} \tag{3}$$

where σ^{o} is the lattice friction stress to dislocation movements and d is the average (sub)grain size, k is a constant. After USSP and natural ageing, d decreases from 2.5 μm to 50 nm. Due to the fact the both the surface layer and substrate in annealed state, thus k value is determined as 30 MPa $\mu m^{0.5}$ according to Fujita and Tabata's work [43]. According to Eq. (3), the increment of strength caused by grain refinement is 115 Mpa.

The usual model used to measure precipitation strengthening of ultrafine grained Al alloy is as follows [44]:

$$\Delta\sigma_p = 0.85M\frac{Gbln(x/b)}{2\pi(L-x)} \tag{4}$$

where x is the average precipitate size and L is the average distance between precipitates. G, b and M are the shear modulus (26 GPa), the Burgers vector of dislocations (0.286 nm for Al) and the Taylor factor (3 for untextured polycrystalline materials), respectively. According to Fig. 8 and Eq. (4), the $\Delta\sigma_p$ = 380 MPa.

Merely considering the effects of Hall–Petch mechanism and Orowan bypass mechanism, the net decrease of hardness is 265 MPa,

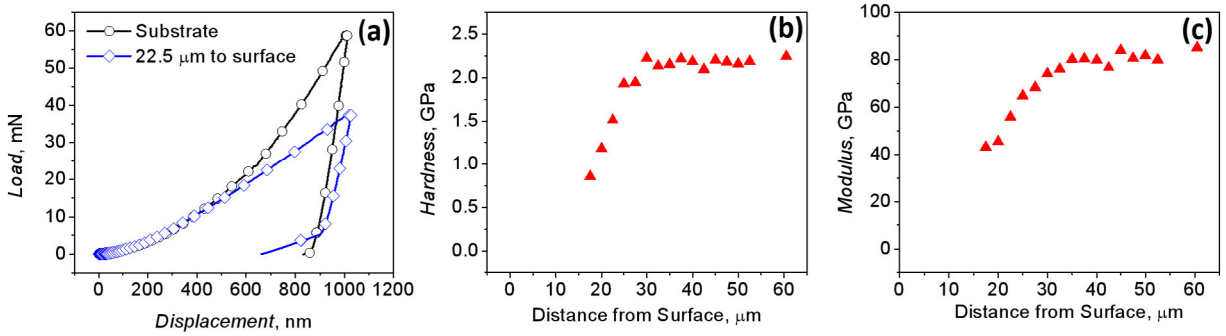

Fig. 11. (a) Load-displacement curves of peened AA 7150; (b) Hardness as a function of distance to surface; (c) Modulus as a function of distance to surface. USSP parameter is U-40 using SiN balls.

which is lower than the actual decline value (~400 MPa). This might be due to the fact that during natural ageing treatment, some voids formed by the annihilation of vacancies which were created by USSP. The presence of voids also is accounted for the decrease in Young's modulus. Therefore, as discussed above, surface softening is mainly due to the fact that softening effect (precipitation coarsening) suppresses grain boundary hardening effects. The low thermal stability of peened sample and natural ageing induced softening behaviour remind us that concerns on of shot peened 7000 series Al alloys during the service life should be raised. In addition, how this low thermal stability affects corrosion performances of peened alloy remains an open question and will be addressed soon by the current group.

5. Conclusion

In summary, an aircraft Al alloy was treated with ultrasonic shot peening, and the corrosion behaviour and thermal stability during natural ageing of which were investigated. Two following conclusions can be drawn from the present study.

1) For the studied environments, corrosion resistance of peened AA7150 is significantly improved compared with its untreated counterpart. For both ND and TD planes which subjected to ultrasonic shot peening, micro-scale intergranular corrosion is completely inhibited in 57 g/L NaCl + 10 mL/L H_2O_2 solution. Exfoliation corrosion sensitivity decreases from EC to EB after ultrasonic shot peening. Pitting potential shifts to the more anodic direction after ultrasonic shot peening, showing a good agreement with exfoliation and intergranular immersion results. Enhanced localized corrosion resistance is believed to be accounted on the formation of equiaxed nano-grains and microstructure homogenization on the surface peened layer.
2) After 1.5 years of natural ageing, coarsen nano-grained precipitates with much larger size than pre-existing η′ and η precipitates, re-precipitate on the peened surface layer. Precipitation coarsening is responsible for surface softening, and concerns on thermal stability of shot peened 7000 series Al alloys during the service life should be raised.

CRediT authorship contribution statement

Qingqing Sun: Validation, Investigation, Resources, Writing - original draft, Writing - review & editing, Conceptualization. **Qingyou Han:** Supervision, Project administration, Funding acquisition. **Shuai Wang:** Writing - review & editing, Visualization, Supervision, Funding acquisition. **Rong Xu:** Writing - review & editing, Methodology.

Declaration of competing interest

The authors declare that they have no known competing financial interests or personal relationships that could have appeared to influence the work reported in this paper.

Acknowledgment

This work was supported by the Center for Technology Development at Purdue University. The financial support of the China Scholarship Council and SUSTech start-up fund are gratefully acknowledged. Project funded by China Postdoctoral Science Foundation (223278) and Youth Innovation Project funded by Education Department of Guangdong Province (2018KQNCX227) are gratefully acknowledged.

References

[1] Y. Estrin, A. Vinogradov, Extreme grain refinement by severe plastic deformation: a wealth of challenging science, Acta Mater. 61 (2013) 782–817.
[2] U. Trdan, J. Grum, SEM/EDS characterization of laser shock peening effect on localized corrosion of Al alloy in a near natural chloride environment, Corros. Sci. 82 (2014) 328–338.
[3] U. Zupanc, J. Grum, Effect of pitting corrosion on fatigue performance of shot-peened aluminium alloy 7075-T651, J. Mater. Process. Technol. 210 (2010) 1197–1202.
[4] Q. Sun, R. Xu, Q. Han, K. Zhao, I. McAdams, W. Xu, Long distance chemical gradient induced by surface nanocrystallization, Appl. Mater. Today 14 (2019) 137–142.
[5] N. Tao, Z. Wang, W. Tong, M. Sui, J. Lu, K. Lu, An investigation of surface nanocrystallization mechanism in Fe induced by surface mechanical attrition treatment, Acta Mater. 50 (2002) 4603–4616.
[6] W. Tong, N. Tao, Z. Wang, J. Lu, K. Lu, Nitriding iron at lower temperatures, Science 299 (2003) 686–688.
[7] P. Chui, K. Sun, C. Sun, X. Yang, T. Shan, Effect of surface nanocrystallization induced by fast multiple rotation rolling on hardness and corrosion behavior of 316L stainless steel, Appl. Surf. Sci. 257 (2011) 6787–6791.
[8] J. Villegas, L. Shaw, K. Dai, W. Yuan, J. Tian, P. Liaw, D. Klarstrom, Enhanced fatigue resistance of a nickel-based hastelloy induced by a surface nanocrystallization and hardening process, Philos. Mag. Lett. 85 (2005) 427–438.
[9] M. Rakita, M. Wang, Q. Han, Y. Liu, F. Yin, Ultrasonic shot peening, Int. J. Comput. Mater. Sci. Surf. Eng. 5 (2013) 189–209.
[10] M. Laleh, F. Kargar, Effect of surface nanocrystallization on the microstructural and corrosion characteristics of AZ91D magnesium alloy, J. Alloys Compd. 509 (2011) 9150–9156.
[11] Q. Sun, X. Liu, Q. Han, J. Li, R. Xu, K. Zhao, A comparison of AA2024 and AA7150 subjected to ultrasonic shot peening: microstructure, surface segregation and corrosion, Surf. Coat. Technol. 337 (2018) 552–560.
[12] R. Waikar, Y. Guo, J. Liu, Z. Liu, Flexible Automation (ISFA), International Symposium on, IEEE, (2016), pp. 359–365.
[13] X. Wu, N. Tao, Y. Hong, B. Xu, J. Lu, K. Lu, Microstructure and evolution of mechanically-induced ultrafine grain in surface layer of AL-alloy subjected to USSP, Acta Mater. 50 (2002) 2075–2084.
[14] Q. Sun, Q. Han, Surface segregation phenomenon of surface severe plastic deformed Al–Zn–Mg–Cu alloys, Materialia 11 (2020) 100741.
[15] B.N. Mordyuk, G.I. Prokopenko, Y.V. Milman, M.O. Iefimov, A.V. Sameljuk, Enhanced fatigue durability of Al–6Mg alloy by applying ultrasonic impact peening: effects of surface hardening and reinforcement with AlCuFe quasicrystalline particles, Mater. Sci. Eng. A 563 (2013) 138–146.
[16] M. Vasylyev, B. Mordyuk, S. Sidorenko, S.M. Voloshko, A.P. Burmak, Peculiarities of structure and phase formation in the surface layers of 2024 aluminium alloy due to ultrasonic impact treatment in various environments, Metallofizika I Noveishie Tekhnologii 39 (2017) 49–68.
[17] U. Trdan, J. Grum, Evaluation of corrosion resistance of AA6082-T651 aluminium alloy after laser shock peening by means of cyclic polarisation and ElS methods, Corros. Sci. 59 (2012) 324–333.
[18] X. Wang, D. Li, Mechanical and electrochemical behavior of nanocrystalline surface of 304 stainless steel, Electrochim. Acta 47 (2002) 3939–3947.
[19] M. Abdulstaar, M. Mhaede, M. Wollmann, L. Wagner, Investigating the effects of bulk and surface severe plastic deformation on the fatigue, corrosion behaviour and corrosion fatigue of AA5083, Surf. Coat. Technol. 254 (2014) 244–251.
[20] J. Pang, F. Liu, J. Liu, M. Tan, D. Blackwood, Friction stir processing of aluminium alloy AA7075: microstructure, surface chemistry and corrosion resistance, Corros. Sci. 106 (2016) 217–228.
[21] X. Liu, G. Frankel, B. Zoofan, S. Rokhlin, Effect of applied tensile stress on intergranular corrosion of AA2024-T3, Corros. Sci. 46 (2004) 405–425.
[22] M. Navaser, M. Atapour, Effect of friction stir processing on pitting corrosion and Intergranular attack of 7075 aluminum alloy, J. Mater. Sci. Technol. 33 (2016) 155–165.
[23] S. Kumar, K. Chattopadhyay, V. Singh, Effect of surface nanostructuring on corrosion behavior of Ti–6Al–4V alloy, Mater. Charact. 121 (2016) 23–30.
[24] S. Jelliti, C. Richard, D. Retraint, T. Roland, M. Chemkhi, C. Demangel, Effect of surface nanocrystallization on the corrosion behavior of Ti–6Al–4V titanium alloy, Surf. Coat. Technol. 224 (2013) 82–87.
[25] T. Balusamy, T.S. Narayanan, K. Ravichandran, I.S. Park, M.H. Lee, Influence of surface mechanical attrition treatment (SMAT) on the corrosion behaviour of AISI 304 stainless steel, Corros. Sci. 74 (2013) 332–344.
[26] Q. Sun, Q. Han, R. Xu, K. Zhao, J. Li, Localized corrosion behaviour of AA7150 after ultrasonic shot peening: corrosion depth vs. impact energy, Corros. Sci. 130 (2018) 218–230.
[27] Q. Sun, Q. Han, X. Liu, W. Xu, J. Li, The effect of surface contamination on corrosion performance of ultrasonic shot peened 7150 Al alloy, Surf. Coat. Technol. 328 (2017) 469–479.
[28] J. Chubb, T. Morad, B. Hockenhull, J. Bristow, The effect of exfoliation corrosion on the fracture and fatigue behaviour of 7178-T6 aluminium, Int. J. Fatigue 17 (1995) 49–54.
[29] T. Marlaud, B. Malki, C. Henon, A. Deschamps, B. Baroux, Relationship between alloy composition, microstructure and exfoliation corrosion in Al–Zn–Mg–Cu alloys, Corros. Sci. 53 (2011) 3139–3149.
[30] X. Zhou, X.Y. Li, K. Lu, Enhanced thermal stability of nanograined metals below a critical grain size, Science 360 (2018) 526.
[31] T. Roland, D. Retraint, K. Lu, J. Lu, Fatigue life improvement through surface

nanostructuring of stainless steel by means of surface mechanical attrition treatment, Scr. Mater. 54 (2006) 1949–1954.
[32] A. Mazilkin, B. Straumal, E. Rabkin, B. Baretzky, S. Enders, S. Protasova, O. Kogtenkova, R. Valiev, Softening of nanostructured Al–Zn and Al–Mg alloys after severe plastic deformation, Acta Mater. 54 (2006) 3933–3939.
[33] B.B. Straumal, B. Baretzky, A.A. Mazilkin, F. Phillipp, O.A. Kogtenkova, M.N. Volkov, R.Z. Valiev, Formation of nanograined structure and decomposition of supersaturated solid solution during high pressure torsion of Al–Zn and Al–Mg alloys, Acta Mater. 52 (2004) 4469–4478.
[34] B. Liu, X. Zhang, X. Zhou, T. Hashimoto, J. Wang, The corrosion behaviour of machined AA7150-T651 aluminium alloy, Corros. Sci. 126 (2017) 265–271.
[35] S.-S. Wang, J.-T. Jiang, G.-H. Fan, A. Panindre, G. Frankel, L. Zhen, Accelerated precipitation and growth of phases in an Al-Zn-Mg-Cu alloy processed by surface abrasion, Acta Mater. 131 (2017) 233–245.
[36] V. Pandey, J.K. Singh, K. Chattopadhyay, N.C.S. Srinivas, V. Singh, Influence of ultrasonic shot peening on corrosion behavior of 7075 aluminum alloy, J. Alloys Compd. 723 (2017) 826–840.
[37] S.-S. Wang, I.-W. Huang, L. Yang, J.-T. Jiang, J.-F. Chen, S.-L. Dai, D.N. Seidman, G. Frankel, L. Zhen, Effect of Cu content and aging conditions on pitting corrosion damage of 7xxx series aluminum alloys, J. Electrochem. Soc. 162 (2015) C150–C160.
[38] Q. Sun, J. Hu, J. Li, K. Chen, P. Dong, X. Liao, Y. Yang, Effect of tempers on electrochemical corrosion behavior of 7150 aluminum alloy plate in various corrosive media, Int. J. Electrochem. Sci. 12 (2017) 5363–5377.
[39] Q. Sun, K. Chen, H. Fang, J. Xu, P. Dong, G. Hu, Q. Chen, Effect of grain refinement on electrochemical behavior of Al–Zn–Mg–Cu alloys, Int. J. Electrochem. Sci. 11 (2016) 5855–5869.
[40] Z. Wang, N. Tao, W. Tong, J. Lu, K. Lu, Diffusion of chromium in nanocrystalline iron produced by means of surface mechanical attrition treatment, Acta Mater. 51 (2003) 4319–4329.
[41] X. Liu, H. Zhang, K. Lu, Strain-induced ultrahard and ultrastable nanolaminated structure in nickel, Science 342 (2013) 337–340.
[42] W. Xu, X.C. Liu, K. Lu, Strain-induced microstructure refinement in pure Al below 100 nm in size, Acta Mater. 152 (2018) 138–147.
[43] H. Fujita, T. Tabata, The effect of grain size and deformation sub-structure on mechanical properties of polycrystalline aluminum, Acta Metall. 21 (1973) 355–365.
[44] S.K. Panigrahi, R. Jayaganthan, Influence of solutes and second phase particles on work hardening behavior of Al 6063 alloy processed by cryorolling, Mater. Sci. Eng. A 528 (2011) 3147–3160.